hydrology

MDPI

Article

Seasonal Variation in Fluorescent Dissolved Organic Matter Composition in Poyang Lake, China

Yiling Zhong [1], Haiqing Liao [1,2,*], Fang Yang [1,2,*], Meng Zhang [2,3], Yuanyan Zhang [2,3], Yule Luo [1], Yuying Shi [1] and Zitong Huang [1]

[1] State Key Laboratory of Environmental Criteria and Risk Assessment, Chinese Research Academy of Environmental Sciences, Beijing 100012, China; 13077243286@139.com (Y.Z.)
[2] Key Laboratory of Protection and Restoration of Yangtze River-Connected Lake (Poyang Lake), Ministry of Ecology and Environment, Nanchang 330099, China
[3] Jiangxi Key Laboratory of Environmental Pollution Control, Jiangxi Academy of Eco-Environmental Sciences & Planning, Nanchang 330099, China
* Correspondence: liaohq@craes.org.cn (H.L.); yang.fang@craes.org.cn (F.Y.)

Abstract

Seasonal hydrological variation can reorganize fluorescent dissolved organic matter (FDOM) in floodplain lakes; yet, its expression in Poyang Lake remains uncertain. We assessed campaign differences in FDOM composition by comparing 32 excitation–emission matrices from 16 fixed sites sampled during the dry and wet periods of 2024 using parallel factor analysis (PARAFAC), fluorescence indices, paired tests with Benjamini–Hochberg correction, and principal component analysis. Rank 4 fitted better and resolved two humic-like and two protein-like regions, although incomplete validation limited component-specific interpretation. In the wet period, C2 and combined humic-like maximum fluorescence intensity (Fmax) decreased (q = 0.00836), whereas bulk total organic carbon (TOC) and total Fmax did not differ. Mean protein-like contribution rose from 25.0% to 37.5% (q = 0.00322); the biological index increased, the humification index decreased, and the fluorescence index was unchanged. The first two principal components explained 78.11% of the variance, and an exact paired multivariate test detected an overall period difference ($p = 3.05 \times 10^{-5}$). No component–environment correlation survived correction or differed between periods. FDOM composition therefore underwent a campaign-specific reorganization without a corresponding change in bulk carbon, but the two-campaign design and incomplete validation preclude causal or source-specific inference.

Keywords: excitation–emission matrices; parallel factor analysis; fluorescence indices; matched-site comparison; humic-like fluorescence; protein-like fluorescence

Check for updates

Academic Editor: Minxue He

Received: 1 July 2026
Revised: 30 July 2026
Accepted: 7 August 2026
Published: 17 August 2026

Copyright: © 2026 by the authors. Licensee MDPI, Basel, Switzerland. This article is an open access article distributed under the terms and conditions of the Creative Commons Attribution (CC BY) license.

1. Introduction

Dissolved organic matter (DOM) is a heterogeneous mixture that participates in aquatic carbon and nutrient cycling, affects light penetration, and interacts with contaminants and trace metals [1,2]. Bulk carbon concentrations alone do not resolve this compositional heterogeneity. Excitation–emission matrix (EEM) fluorescence spectroscopy provides rapid information on the fluorescent fraction of DOM (FDOM), while parallel factor analysis (PARAFAC) separates a collection of EEMs into latent excitation and emission profiles and sample scores [3–6]. Fluorescence index (FI), biological index (BIX), and humification index (HIX) offer additional operational descriptors of FDOM character. However, these indices and PARAFAC components represent optical patterns rather than unique

compounds or source tracers, and their interpretation depends on instrument settings, preprocessing, calibration, and model validation [7–11]. They should therefore be interpreted together with supporting environmental evidence rather than used alone to establish DOM sources or processes.

Seasonal EEM-PARAFAC studies in lakes and rivers have documented changes in both humic-like and protein-like fluorescence, but the magnitude and direction of those changes differ among climatic and hydrological settings. Seasonal comparisons in alpine lake-stream networks, semiarid lakes, and monsoonal rivers illustrate that similar fluorescence regions can vary differently among systems [12–14]. These differences make study design and model evaluation important. Resampling the same sites can reduce confounding between spatial heterogeneity and sampling period, while comparison of plausible PARAFAC ranks can show whether a conclusion depends on a particular component partition. Likewise, a correlation detected in one sampling period but not another does not by itself demonstrate that the correlations differ; the contrast must be tested directly [15].

Poyang Lake is a large, seasonally dynamic floodplain lake connected to the Yangtze River and supplied by five major tributaries. Its floodplain depressions alternate between connection and isolation as water levels change, creating spatially variable exchange conditions across the lake system [16,17]. Changes in water level and inundated area therefore provide essential regional context for interpreting water-quality, but DOM in this system has already been examined from several complementary perspectives. Previous studies have related historical water-quality variation to hydrological conditions and DOM fluorescence [18], described the spatial distribution and optical properties of chromophoric DOM (CDOM) [19], and characterized fractionated FDOM in the five tributaries [20]. Separate regional analyses have also associated land-use composition in multi-scale buffer zones with spatial and temporal variation in lake water-quality [21]. More recent DOM research has examined CDOM and dissolved organic carbon over four hydrological periods [22], evaluated multi-year spatial–seasonal patterns [23], and combined optical spectroscopy with Fourier-transform ion cyclotron resonance mass spectrometry to characterize molecular heterogeneity [24,25]. A newly published regional study further treated winter–drought and summer–flood conditions as coupled hydroclimatic states when evaluating CDOM optical proxies [26]. Thus, neither seasonal DOM variation nor its regional hydrological context is new to Poyang Lake, and the present study is not positioned as the first lake-wide DOM investigation.

This study compares fluorescent dissolved organic matter at 16 fixed locations sampled in March and August 2024. Three- and four-component PARAFAC models, paired comparisons of fluorescence components and indices, component–environment correlations, and principal component analysis were used to characterize seasonal differences in optical composition. The analysis evaluates the two campaigns as contrasting seasonal periods; daily water levels at Xingzi provide lake-scale hydrological context, whereas site-scale hydrological controls were not evaluated.

Accordingly, this study addresses three questions: (1) what broad fluorescence structure is recovered from the 32 EEMs, and how sensitive is that structure to selection of a three- or four-component PARAFAC model; (2) which component intensities, relative contributions, and fluorescence indices differ between the two matched sampling periods; and (3) do the multivariate optical characteristics and component–environment relationships differ between periods? We hypothesized that the contrasting dry- and wet-period settings would be associated with differences in FDOM composition at matched sites, without necessarily implying a corresponding change in bulk TOC.

2. Materials and Methods

2.1. Study Area and Sampling Design

Poyang Lake (28°24′–29°46′ N, 115°49′–116°46′ E) is a large floodplain lake in northern Jiangxi Province in the middle–lower Yangtze River basin. The lake receives inflow from the Gan, Fu, Xin, Rao, and Xiu Rivers and is connected to the Yangtze River through its northern outlet. Geologically, the lacustrine plain and adjacent riparian floodplains are underlain mainly by Quaternary unconsolidated deposits. The principal geological units comprise Holocene, upper Pleistocene, and middle–lower Pleistocene unconsolidated deposits formed in fluvial and lacustrine settings [27]. The basin has a humid subtropical monsoon climate with pronounced seasonal precipitation, and lake water level and inundated area vary markedly between the high- and low-water periods. Long-term remote-sensing records show that lake area is generally smallest in winter and largest in summer. Across 1989–2018, annual water-area extrema ranged from 899.68 km^2 in 2014 to 4068.33 km^2 in 1998, illustrating the magnitude of long-term surface-area variation; these values are regional context rather than estimates for the two 2024 sampling dates [28]. At a lake-mouth water level of 21.71 m, the mean lake depth has been reported as 8.4 m [28], and the deepest point is approximately 25.1 m [29]. Hydrodynamic studies further indicate that approximately 85% of the flood-period lake area is shallower than 6 m and that vertical temperature and velocity stratification is generally weak [30]. A modeled mean residence time of 89 days for July–September has been reported, although transport and retention vary among the main channels and bays [30]. Seasonal connection and isolation of floodplain depressions also create spatially variable exchange conditions and water-quality patterns [16,17]. Monitoring from 2018 to 2020 characterized Poyang Lake as having a medium-to-rich nutrient level, while showing that eutrophic conditions occurred in some areas in every month and that nutrient conditions varied between lake regions and hydrological periods [31]. Long-term water-quality assessment likewise identified nitrogen and phosphorus as major pressures [32]. The surrounding basin contains cropland, forest, water, and built-up land, and land-use–water-quality relationships vary with buffer scale [21]. These published characteristics provide regional context rather than measurements from the 2024 campaigns. A single trophic class was not assigned to the 2024 samples because a complete campaign-specific trophic-level-index dataset was unavailable; synchronous site-specific hydrological observations, site-specific land-use data, and mixing profiles were also unavailable and were not used as explanatory variables.

Daily water levels at Xingzi station were obtained from the Department of Ecology and Environment of Jiangxi Province to describe the hydrological setting of the two campaigns. Values in March 2024 ranged from 9.94 to 11.97 m (10.89 $\pm$ 0.76 m, n = 31), compared with 14.92 to 19.19 m in August 2024 (17.25 $\pm$ 1.28 m, n = 31). The non-overlapping monthly ranges characterize the two campaigns as low- and high-water periods at the lake scale.

Surface-water samples were collected at the same 16 fixed sampling sites (S1–S16) in March and August 2024, representing the dry- and wet-period campaigns, respectively (Figure 1). Each site was revisited in both campaigns, and period comparisons therefore used a matched-site design. The sites were not assigned to tributary-mouth, shoreline, or lake-center classes because a reproducible site-classification scheme was unavailable. One sample was analyzed at each site in each campaign, giving 32 site-period samples in total. Fixed-site coordinates and retained field water-depth observations are presented in Table 1.

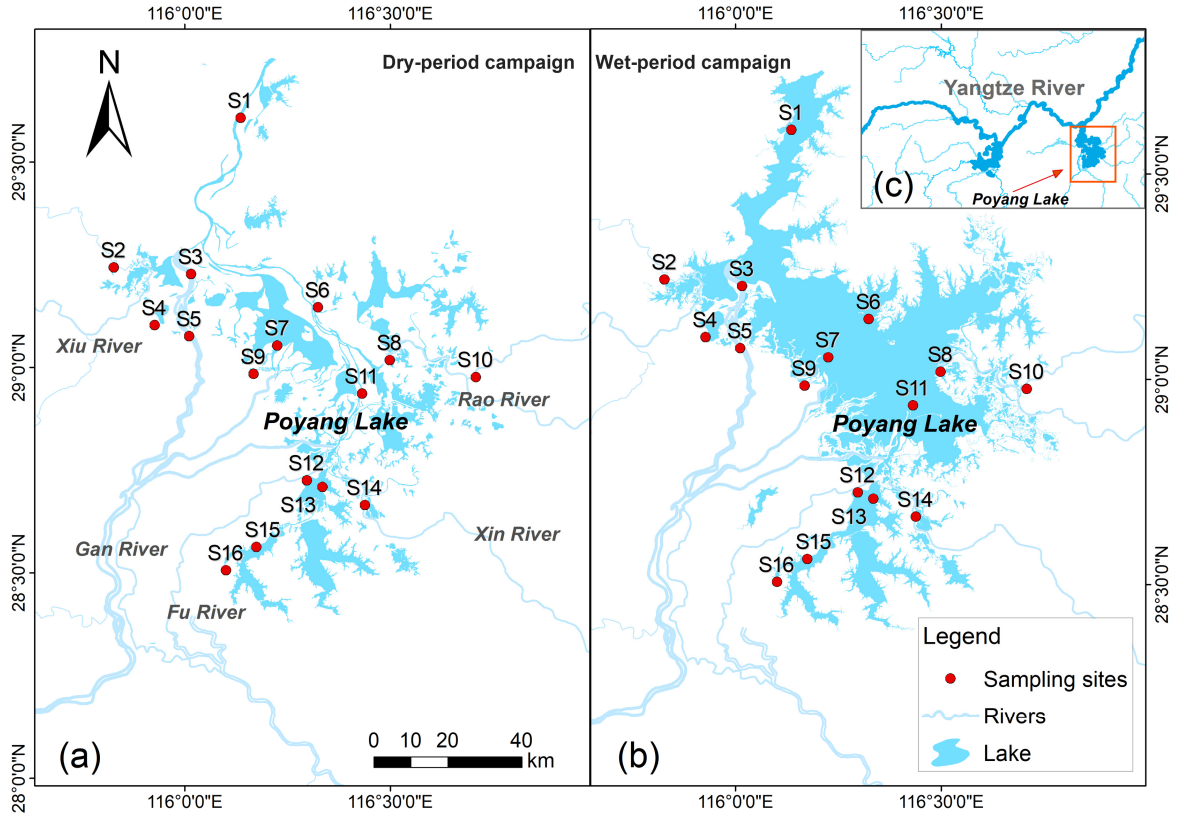


Figure 1. Sampling-site maps for the two campaigns and regional location: (**a**) dry-period campaign, showing the 16 fixed sampling sites; (**b**) wet-period campaign, showing the same 16 fixed sampling sites; and (**c**) the location of Poyang Lake and its northern connection to the Yangtze River. The two panels reproduce the lake outlines shown in the archived sampling map. Because the source dates and processing metadata of these outlines were unavailable, they are presented only as schematic geographic context and were not quantified or analyzed as hydrological variables. Sampling sites are not assigned to tributary-mouth, shoreline, or lake-center classes because no predefined, reproducible site-classification metadata were archived.

Table 1. Fixed-site coordinates and available field water-depth observations.

Site	Longitude (°E)	Latitude (°N)	Dry Depth (m)	Wet Depth (m)
S1	116.1359	29.6081	9.5	8.2
S2	115.8275	29.2436	NR	NR
S3	116.0155	29.2277	5.7	12.4
S4	115.9270	29.1033	NR	NR
S5	116.0113	29.0763	NR	NR
S6	116.3238	29.1468	3.7	2.5
S7	116.2254	29.0539	NR	3.4
S8	116.4986	29.0184	4.0	4.0
S9	116.1675	28.9847	NR	NR
S10	116.7078	28.9768	11.4	13.2
S11	116.4314	28.9368	2.9	5.3
S12	116.3351	28.7094	3.7	1.9
S13	116.2973	28.7251	2.3	8.1

Table 1. *Cont.*

Site	Longitude (°E)	Latitude (°N)	Dry Depth (m)	Wet Depth (m)
S14	116.4381	28.6655	NR	NR
S15	116.1746	28.5629	NR	NR
S16	116.1008	28.5066	NR	NR

Coordinates are the common fixed-site reference used for both campaigns. NR indicates that no retained field-depth record was available for that campaign.

2.2. Water-Quality Measurements

Water temperature, oxidation-reduction potential (ORP), dissolved oxygen (DO), pH, and electrical conductivity (EC) were recorded in situ. The available methods documentation identified an HQ40d portable multiparameter meter (Hach, Loveland, CO, USA), although probe-specific metadata were unavailable. Water depth and transparency were recorded where available. Laboratory variables comprised total organic carbon (TOC), total nitrogen (TN), nitrate nitrogen (NO_3^-–N), ammonia nitrogen (NH_4^+–N), and chlorophyll *a* (chl-*a*). TOC was determined by high-temperature combustion oxidation–nondispersive infrared detection using the difference method (TOC = TC − IC), following HJ 501-2009 [33]. TN was determined by alkaline potassium persulfate digestion followed by UV spectrophotometry, following HJ 636-2012 [34]. NO_3^-–N was measured by UV spectrophotometry following HJ/T 346-2007 [35], and ammonia nitrogen, reported as NH_4^+–N, was measured by Nessler's reagent spectrophotometry following HJ 535-2009 [36]. Chl-*a* was quantified spectrophotometrically after 90% acetone extraction using absorbances at 750, 663, 645, and 630 nm, following the method described in *Water and Wastewater Monitoring and Analysis Methods* (4th ed.) [37]. Water depth was treated as a local, single-occasion field descriptor rather than a measure of lake-scale water level.

The filtration status of the aliquot used for TOC analysis could not be verified. The carbon variable is therefore reported as bulk TOC and is not relabeled as dissolved organic carbon. Chl-*a* was available for eight dry-period sites (n = 8) and all 16 wet-period sites (n = 16); other variable-specific sample sizes are reported in the corresponding tables. Missing observations were not imputed.

2.3. Eem Acquisition and Preprocessing

Aliquots used for fluorescence analysis were passed through 0.45 μm filters; the filter material was not recorded. Excitation–emission matrices (EEMs) were acquired using a Hitachi F-7000 spectrofluorometer (Hitachi, Tokyo, Japan). The common analysis range was 200–450 nm for excitation and 260–550 nm for emission, both at 5 nm intervals. The recorded scan speed was 12,000 nm min^{-1}, and the excitation and emission slit widths were 5 nm.

An ultrapure-water blank was subtracted from the sample EEMs, and negative blank-subtracted values were set to zero. First- and second-order Rayleigh and Raman scatter bands were masked and treated as missing values, rather than replaced with zeros, during model fitting. The analysis preserved the NaN scatter mask in the archived processed EEM cube; exact mask-band widths could not be reconstructed from the retained files. The final EEM cube contained 32 samples × 59 emission wavelengths × 51 excitation wavelengths, with 19,072 values masked. No dilution records were available. The processing files contained no absorbance-based inner-filter-effect correction, Raman-area normalization, or instrument-response correction. Because these procedures affect fluorescence comparability and inner-filter bias [8,38], PARAFAC maximum fluorescence values (Fmax) are reported in arbitrary units (a.u.) and are interpreted only as internally comparable values within this dataset.

2.4. Fluorescence Indices

The fluorescence index (FI), biological index (BIX), and humification index (HIX) were recalculated directly from the processed EEM cube after verification of the sample-to-site mapping. Before peak extraction, EEMs were interpolated to 1 nm intervals, and emission scans were smoothed using a 21-point, second-order Savitzky–Golay procedure implemented in the archived drEEM PickPeaks workflow (v0.1.0). FI was originally introduced by McKnight et al. [39], and the 470/520 nm formulation described by Cory and McKnight [7] was used here. The implemented definitions were:

- FI = I(Ex 370 nm, Em 470 nm)/I(Ex 370 nm, Em 520 nm);
- BIX = I(Ex 310 nm, Em 380 nm)/I(Ex 310 nm, Em 430 nm) [40]; and
- HIX = ΣI(Ex 254 nm, Em 435–480 nm)/[ΣI(Ex 254 nm, Em 300–345 nm) + ΣI(Ex 254 nm, Em 435–480 nm)] [41].

Because Raman normalization and instrument-response correction were unavailable, the indices were used as operational within-dataset descriptors. Absolute FI source thresholds derived from calibrated datasets were not applied. The recalculated FI, BIX, and HIX values are therefore interpreted only as internally comparable optical descriptors.

2.5. Parafac Modeling and Validation

PARAFAC models were fitted to the combined 32-sample EEM cube in MATLAB R2024b (MathWorks, Natick, MA, USA) using DOMFluor/N-way routines [42]. Non-negativity constraints were imposed on the sample, emission, and excitation modes, and the convergence tolerance was 10^{-6}. Three- and four-component models were each fitted from 10 random initializations, with the minimum-SSE solution retained for evaluation. Model fit was compared using the sum of squared errors (SSE), root-mean-square error (RMSE), and explained variance. Structural diagnostics included core consistency and random-start stability [43].

Component-specific sample loadings from the scaled PARAFAC solution were treated as Fmax. For component i, the relative contribution was calculated as $Fmax_i/\Sigma Fmax(C1–C4) \times 100\%$. In the rank-4 solution, C1 + C2 defined the combined humic-like signal and C3 + C4 defined the combined protein-like signal.

Four split cubes were generated from the 32-sample dataset using the drEEM toolbox (v0.1.0), including its 'SplitData' routine [6]. Split-half validation then used two independent comparisons: Split 1 versus Split 2 and Split 3 versus Split 4. For each split and each model rank, 10 random initializations were fitted and the minimum-SSE solution was retained. Components were aligned by jointly maximizing excitation and emission similarity. A component match passed the strict split-half criterion only when both excitation and emission Tucker congruence coefficients were at least 0.95 [44]. Observed, reconstructed, and residual EEMs were also generated for every sample and model rank. Model selection was based on the combined fit and validation evidence rather than explained variance alone.

Published comparisons show that broad fluorescence regions recur across natural and engineered waters, while also cautioning that similar spectra need not imply identical chemistry [3,7,9]. Component classes were assigned from their excitation and emission maxima and direct comparison with published fluorescence regions [6,45–48], rather than from an online spectral-library match. The rank-4 solution was described as two broad humic-like and two broad protein-like fluorescence regions, and the protein-like components were not treated as unique compounds or source-specific tracers. A rank-3/rank-4 sensitivity analysis tested whether the combined humic-like and protein-like period contrasts depended on separating the two protein-like regions.

The component characteristics and implemented fluorescence-index definitions are summarized in Table 2.

Table 2. Spectral characteristics of the PARAFAC components and fluorescence-index definitions.

Metric	Spectral Definition	Broad Interpretation	Validation/Processing Note	Supporting Literature
C1	Ex/Em = 265/440 nm	Humic-like fluorescence	Strongest class-level spectral support	[6,47]
C2	Ex/Em = 235/420 nm	Short-wavelength humic-like fluorescence	Moderate spectral support	[6,45]
C3	Ex maxima near 220 and 280 nm; Em maximum near 315 nm	Protein-like fluorescence region	Weak split-half support; avoid source-specific attribution	[46,48]
C4	Ex maximum near 235 nm with a longer-wavelength shoulder; Em maximum near 340 nm	Protein-like fluorescence region	Weak split-half support; interpret with C3 where possible	[6,46]
FI	Ex 370 nm; Em 470/520 nm	Relative variation in fluorescence spectral shape	1 nm interpolation; 21-point, second-order Savitzky–Golay smoothing; no absolute source thresholds	[7,39]
BIX	Ex 310 nm; Em 380/430 nm	Fresh/autochthonous-like optical signal	Same interpolation and smoothing workflow	[40]
HIX	Ex 254 nm; ΣEm435–480/(ΣEm300–345 + ΣEm435–480)	Relative humification-related optical signal	Same interpolation and smoothing workflow	[41]

2.6. Statistical and Sensitivity Analyses

Variables were summarized by sampling period using sample size, mean ± standard deviation, and range. Because the same 16 fixed sites were revisited, period differences were evaluated using exact paired Wilcoxon signed-rank tests. Exact p values, BH-adjusted q values, and rank-biserial correlations are reported in the main comparison tables. Benjamini–Hochberg (BH) correction was applied separately to 12 environmental tests, 16 optical tests, and 5 TOC-normalized tests [49]. Statistical conclusions were based on BH-adjusted $q < 0.05$.

Within each period, Spearman correlations were calculated between C1–C4 Fmax and eight environmental variables: TOC, TN, NO_3^-–N, NH_4^+–N, chl-*a*, DO, pH, and EC. Pairwise-complete observations were used, and BH adjustment was applied across the 32 component–environment correlations within each period. The occurrence of a significant correlation in one period and a nonsignificant correlation in the other was not treated as evidence that the correlations differed. Instead, dry–wet differences in each Spearman coefficient were tested directly using an exact paired permutation procedure that exchanged the period labels within each paired site identifier and used the absolute difference in correlation coefficients as the test statistic. These 32 direct correlation-difference tests formed a separate BH family. The number of permutations was 2^n for the sites with complete paired observations.

Principal component analysis (PCA) was applied to C1–C4 Fmax, FI, BIX, and HIX. Fmax variables were log10-transformed, and all seven variables were standardized using the combined 32-sample mean and standard deviation. An exact paired multivariate permutation test used all 2^{16} within-site sign reversals to evaluate the overall period shift in the standardized optical vector; the test statistic was the squared Euclidean norm of the mean paired-difference vector. Exploratory spatial analysis tested Spearman associations of

PC1 and PC2 scores with latitude and longitude using one common coordinate for each of the 16 fixed sampling sites. Regional group tests were not conducted because no predefined hydrogeomorphic or site-type classification was available and the seasonally changing shoreline made a post hoc visual classification non-reproducible. Redundancy analysis was not applied because this dataset—16 observations per campaign, correlated predictors, and incomplete chl-*a* data—was not considered adequate for a defensible constrained model. Kriging was not attempted because this sampling design did not permit defensible variogram estimation and validation for a spatially complex lake.

As a secondary sensitivity analysis, Fmax values were normalized to bulk TOC to examine whether seasonal patterns persisted when expressed relative to the measured carbon pool [50,51]. These ratios were treated as operational carbon-normalized fluorescence intensities, rather than as quantitative fluorescence yields or source contributions; TOC was excluded from correlations involving normalized variables to avoid denominator coupling. The unusually high dry-period C4 value at S2 was retained in the primary analysis, and its influence was assessed by a paired sensitivity analysis.

3. Results

3.1. Environmental Conditions

Water temperature, pH, and TN differed between periods after BH correction (Table 3). No adjusted differences were detected for the remaining environmental variables, including field water depth, transparency, TOC, NO_3^-–N, NH_4^+–N, and chl-*a*. Although local water depth did not differ between campaigns, lake-scale water levels at Xingzi were higher during the August campaign. Complete descriptive statistics and paired comparisons are presented in Table 3.

Table 3. Environmental and water-quality conditions during the two sampling campaigns.

Variable	Dry *n*	Dry Mean ± SD	Dry Range	Wet *n*	Wet Mean ± SD	Wet Range	Paired *n*	Exact *p*	BH q	Rank-Biserial Effect
Water temperature (°C)	16	20.60 ± 2.54	17.34–25.98	16	33.43 ± 1.14	30.62–35.31	16	<0.0001	0.0004	1.000
Oxidation-reduction potential (mV)	16	240.69 ± 88.13	110.90–393.00	16	204.55 ± 35.36	147.50–299.00	16	0.2114	0.4688	−0.368
pH	16	7.43 ± 0.87	6.44–9.35	16	8.35 ± 0.61	7.58–9.35	16	0.0042	0.0206	0.779
Electrical conductivity ($\mu S\,cm^{-1}$)	16	116.02 ± 54.05	36.00–205.50	16	128.75 ± 70.94	37.00–316.00	16	0.4543	0.6814	0.233
Dissolved oxygen ($mg\,L^{-1}$)	16	6.62 ± 2.96	2.34–11.14	16	6.37 ± 0.84	4.81–8.63	16	0.8209	0.8955	−0.074
Water depth (m)	8	5.40 ± 3.31	2.30–11.40	9	6.56 ± 4.18	1.90–13.20	8	0.2344	0.4688	0.500
Transparency (m)	8	0.48 ± 0.17	0.35–0.88	16	0.44 ± 0.27	0.08–1.10	8	0.7891	0.8955	0.139
TOC ($mg\,L^{-1}$)	16	2.75 ± 0.82	1.94–4.54	16	2.70 ± 0.89	1.89–5.18	16	0.4037	0.6814	−0.250
TN ($mg\,L^{-1}$)	16	1.55 ± 0.43	0.93–2.61	16	2.13 ± 0.48	1.15–2.68	16	0.0052	0.0206	0.765
NO_3^-–N ($mg\,L^{-1}$)	16	0.83 ± 0.32	0.19–1.63	16	0.86 ± 0.37	0.32–1.47	16	0.8999	0.8999	0.044
NH_4^+–N ($mg\,L^{-1}$)	16	0.24 ± 0.06	0.15–0.35	16	0.33 ± 0.31	0.12–1.33	16	0.6322	0.8429	0.147
Chlorophyll *a* ($mg\,m^{-3}$)	8	10.12 ± 4.98	3.75–17.40	16	6.52 ± 5.32	1.00–22.32	8	0.0391	0.1172	−0.833

Notes: Values are site-level observations. Seasonal comparisons used exact paired Wilcoxon signed-rank tests; BH q values were adjusted across the 12 environmental tests. Rank-biserial effects are positive for wet > dry.

3.2. Parafac Model and Validation

The rank-4 solution comprised two humic-like and two protein-like fluorescence regions (Figure 2; Table 2). C1 and C2 had excitation/emission maxima at 265/440 and 235/420 nm, respectively. C3 showed excitation maxima near 220 and 280 nm and an emission maximum at 315 nm. C4 had an excitation maximum near 235 nm, a longer-wavelength shoulder near 280 nm, and an emission maximum at 340 nm. The component labels refer to broad fluorescence regions rather than unique compounds or sources.

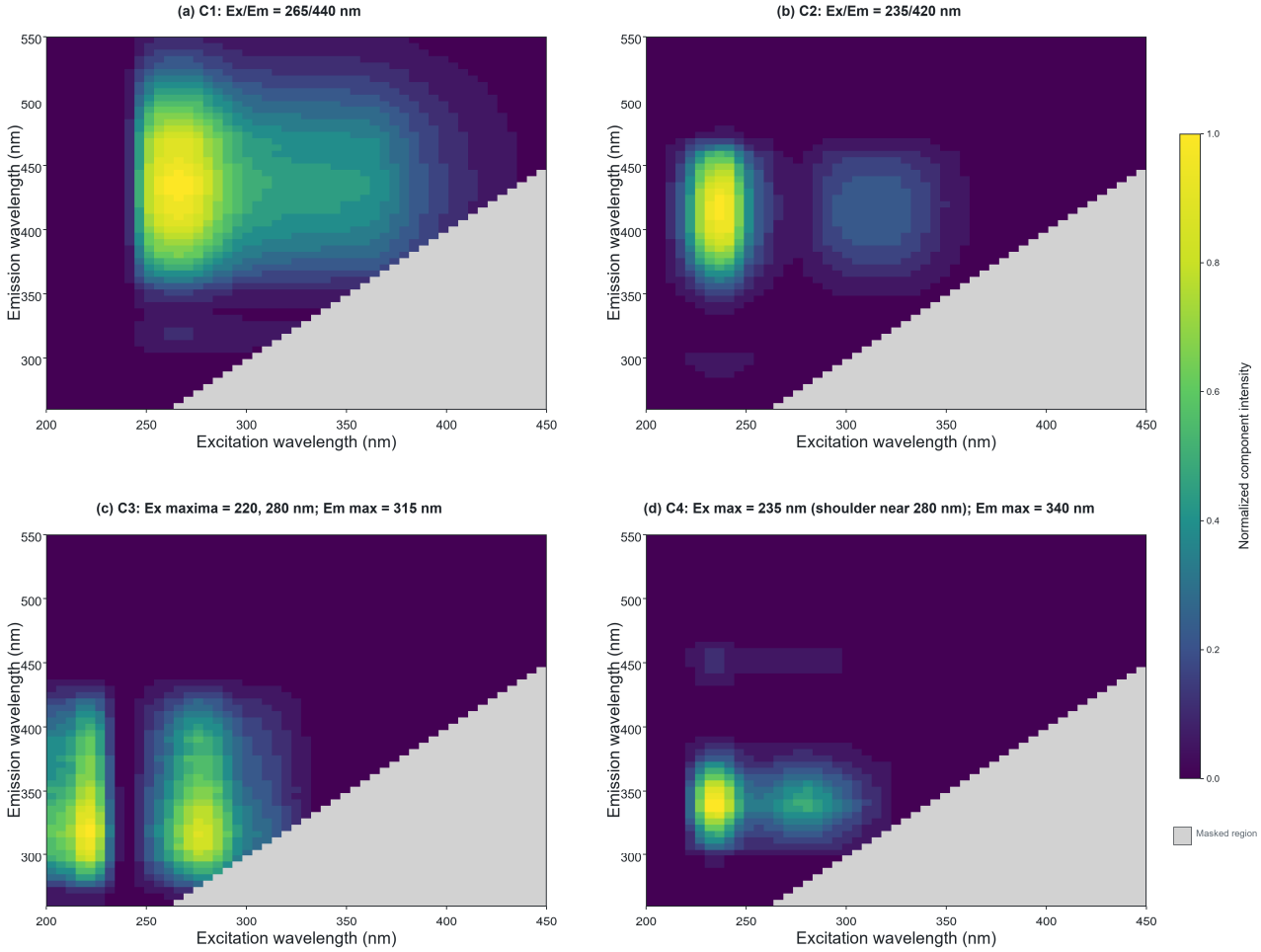


Figure 2. Normalized excitation–emission surfaces of the four-component PARAFAC solution: (**a**) C1, humic-like; (**b**) C2, humic-like; (**c**) C3, protein-like; and (**d**) C4, protein-like. Excitation wavelength is shown on the x-axis and emission wavelength on the y-axis. Intensities are normalized to the maximum of each component and therefore range from 0 to 1; gray denotes the masked scattering region. C3 has excitation maxima near 220 and 280 nm, and C4 has an excitation maximum near 235 nm with a shoulder near 280 nm. Rank 4 provided the better descriptive fit, but split-half support for C3 and C4 was weak; these components are therefore interpreted as broad protein-like fluorescence regions rather than source-specific tracers.

Compared with rank 3, rank 4 reduced SSE from 66.01 $\times$ 10^6 to 39.27 $\times$ 10^6 and RMSE from 29.24 to 22.55, while explained variance increased from 97.084% to 98.265%. Core consistency was lower for rank 4 (38.8%) than for rank 3 (57.8%). The rank-4 random-start solutions were highly reproducible: all 10 starts met the excitation/emission congruence criterion relative to the best solution, and the SSE spread was 0.000439%.

Split-half support was uneven. Only three of the eight matched rank-4 component comparisons met the strict criterion of excitation and emission Tucker congruence coefficients $\geq$0.95; none of the six rank-3 comparisons met both thresholds. Rank 4 was retained

because it fitted the EEM data better and was stable across random starts, but the weaker split-half support limits component-specific interpretation, particularly for C3 and C4. The class-level seasonal change occurred in both rank solutions.

3.3. Seasonal Optical Variation and Multivariate Separation

Among the component intensities, C2 showed the clearest seasonal difference (Table 4). Median C2 Fmax decreased from 480.8 a.u. in the dry period to 329.1 a.u. in the wet period (p = 0.00418, q = 0.00836). The combined humic-like Fmax also decreased (q = 0.00836). C1, C3, C4, total Fmax, and combined protein-like Fmax did not differ after correction; for combined protein-like Fmax, p = 0.0443 and q = 0.0709.

Table 4. Seasonal comparison of DOM optical properties.

Variable	Dry *n*	Dry Mean ± SD	Dry Range	Wet *n*	Wet Mean ± SD	Wet Range	Paired *n*	Exact *p*	BH q	Rank-Biserial Effect
C1 Fmax (a.u.)	16	357.32 ± 88.65	212.93–592.85	16	310.37 ± 101.72	168.92–530.73	16	0.0577	0.0769	−0.544
C2 Fmax (a.u.)	16	490.66 ± 125.00	270.66–795.43	16	348.58 ± 160.67	130.17–639.97	16	0.0042	0.0084	−0.779
C3 Fmax (a.u.)	16	105.04 ± 32.95	52.99–204.45	16	193.08 ± 195.61	46.62–854.36	16	0.0507	0.0737	0.559
C4 Fmax (a.u.)	16	225.35 ± 314.36	79.09–1362.14	16	243.89 ± 139.78	89.46–482.61	16	0.0739	0.0910	0.515
Total Fmax (a.u.)	16	1178.38 ± 483.70	615.68–2637.02	16	1095.92 ± 515.36	436.11–2293.71	16	0.4637	0.4637	−0.221
Combined humic-like Fmax (a.u.)	16	847.99 ± 210.94	483.59–1388.28	16	658.95 ± 259.94	299.09–1170.70	16	0.0042	0.0084	−0.779
Combined protein-like Fmax (a.u.)	16	330.39 ± 343.11	132.09–1566.59	16	436.97 ± 301.43	137.02–1336.82	16	0.0443	0.0709	0.574
C1 relative contribution (%)	16	31.77 ± 4.79	15.49–35.38	16	30.37 ± 5.83	17.96–40.24	16	0.4332	0.4637	−0.235
C2 relative contribution (%)	16	43.27 ± 5.11	25.10–46.94	16	32.12 ± 4.97	23.76–41.82	16	<0.0001	0.0003	−0.985
C3 relative contribution (%)	16	9.24 ± 1.73	6.49–12.47	16	15.36 ± 7.61	7.42–37.25	16	0.0013	0.0035	0.853
C4 relative contribution (%)	16	15.72 ± 10.02	10.38–51.65	16	22.15 ± 6.50	11.32–36.54	16	0.0076	0.0136	0.735
Combined humic-like contribution (%)	16	75.04 ± 9.66	40.59–81.46	16	62.49 ± 9.01	41.72–75.46	16	0.0010	0.0032	−0.868
Combined protein-like contribution (%)	16	24.96 ± 9.66	18.54–59.41	16	37.51 ± 9.01	24.54–58.28	16	0.0010	0.0032	0.868
Fluorescence index (FI)	16	2.39 ± 0.07	2.28–2.51	16	2.41 ± 0.06	2.33–2.50	16	0.4637	0.4637	0.221
Biological index (BIX)	16	0.82 ± 0.03	0.78–0.90	16	1.03 ± 0.04	0.95–1.11	16	<0.0001	0.0003	1.000
Humification index (HIX)	16	0.82 ± 0.07	0.56–0.86	16	0.68 ± 0.06	0.53–0.75	16	<0.0001	0.0003	−0.985

Notes: Values are site-level observations. Seasonal comparisons used exact paired Wilcoxon signed-rank tests; BH q values were adjusted across the 16 optical tests. Rank-biserial effects are positive for wet > dry.

Changes in relative composition were more marked (Figure 3). The mean humic-like contribution decreased from 75.0% to 62.5%, while the protein-like contribution increased from 25.0% to 37.5% (both q = 0.00322). C2 declined from 43.3% to 32.1% (q = 0.000326). C3 increased from 9.24% to 15.36% (q = 0.00350), and C4 increased from 15.72% to 22.15% (q = 0.0136). C1 showed no significant proportional change.

Mean BIX increased from 0.818 ± 0.033 to 1.031 ± 0.043 (q = 0.000326), whereas mean HIX decreased from 0.816 ± 0.069 to 0.681 ± 0.055 (q = 0.000326; Figure 4; Table 4). FI was similar in the dry and wet periods (2.390 ± 0.072 and 2.413 ± 0.064, respectively; $p = q$ = 0.464).

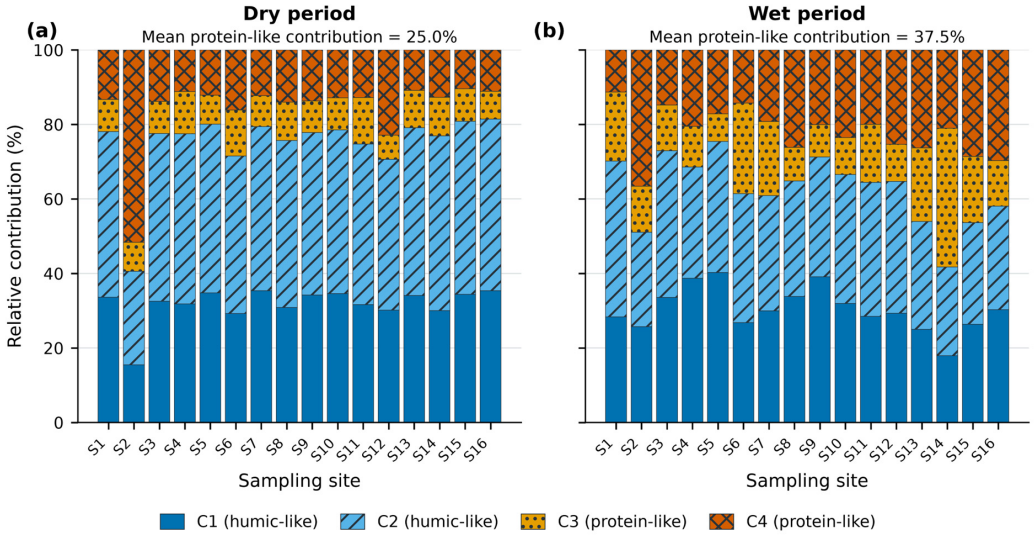


Figure 3. Relative contributions of the four PARAFAC components at 16 matched sampling sites during the (**a**) dry and (**b**) wet periods. Colors and hatching identify C1–C4; C1 and C2 are humic-like components, whereas C3 and C4 are protein-like components. The mean combined protein-like contribution increased from 25.0% in the dry period to 37.5% in the wet period (exact paired Wilcoxon $p = 0.001007$; BH-adjusted $q = 0.00322$). Site S2, which had an unusually high dry-period C4 contribution, is retained as an observed value and evaluated in the sensitivity analysis.

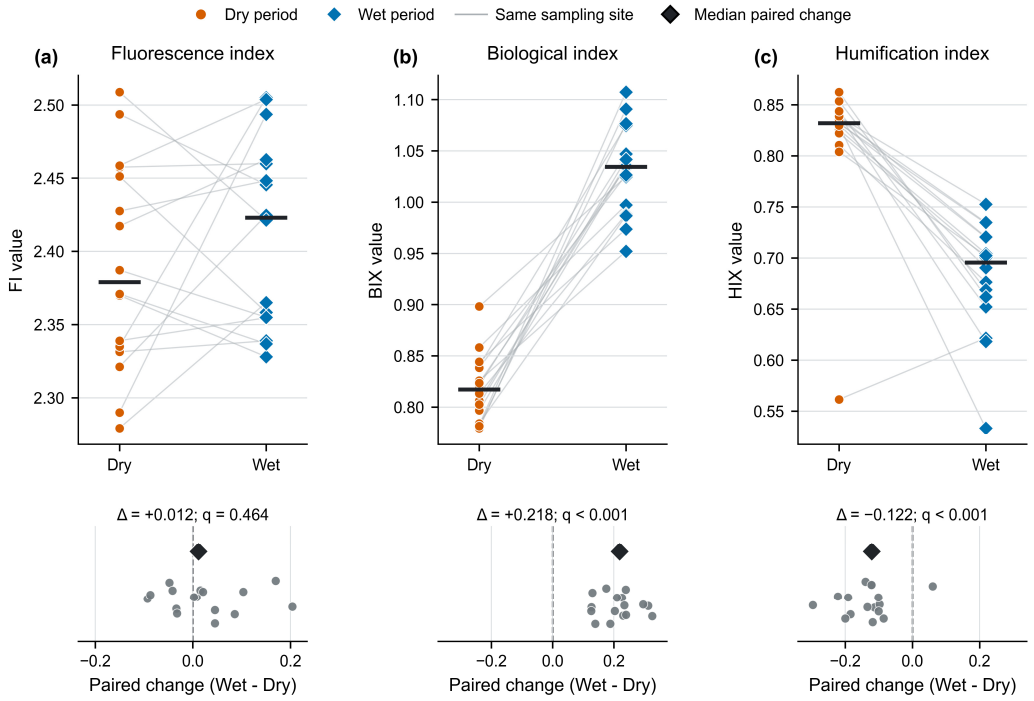


Figure 4. Paired site-level fluorescence indices during the dry and wet sampling periods: (**a**) fluorescence index (FI), (**b**) biological index (BIX), and (**c**) humification index (HIX). In the upper panels, lines connect measurements from the same sampling site, circles and diamonds denote dry- and wet-period observations, respectively, and horizontal black bars indicate medians ($n = 16$ matched sites). The lower panels show individual paired differences (wet minus dry); black diamonds indicate the median paired difference. FI did not differ between periods (exact paired Wilcoxon $p = 0.464$; BH-adjusted $q = 0.464$), whereas BIX increased ($p = 3.05 \times 10^{-5}$; $q = 0.000326$) and HIX decreased ($p = 6.10 \times 10^{-5}$; $q = 0.000326$). Indices were recalculated directly from the archived EEM cube and are used as within-dataset operational descriptors.

The first two principal components accounted for 78.11% of the variance in C1–C4 Fmax, FI, BIX, and HIX (PC1, 43.99%; PC2, 34.12%; Figure 5). Scores differed between the paired dry- and wet-period samples in the exact multivariate permutation test ($p = 3.05 \times 10^{-5}$; 65,536 permutations).

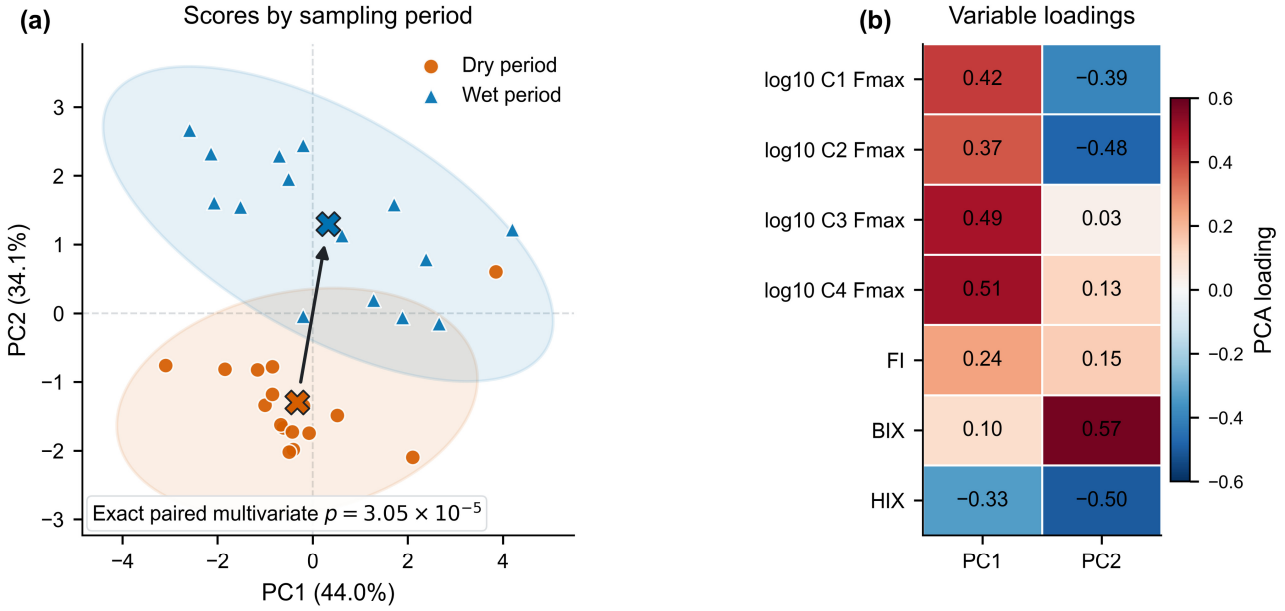


Figure 5. Principal component analysis of log10-transformed C1–C4 Fmax values and FI, BIX, and HIX values. (**a**) Sample scores on PC1 and PC2, which explained 43.99% and 34.12% of the total variance, respectively. Colors and marker shapes identify sampling periods; shaded regions are 95% covariance ellipses, X symbols are group centroids, and the arrow shows the shift from the dry-period centroid to the wet-period centroid. An exact paired multivariate permutation test detected an overall between-period difference ($p = 3.05 \times 10^{-5}$; 65,536 permutations). (**b**) Loadings of the seven optical variables on PC1 and PC2. Positive and negative loadings are shown by a zero-centered diverging color scale and printed numerically.

Spearman tests using the common coordinates for the 16 fixed sites found no adjusted relationship between PC1 or PC2 and latitude or longitude. The lowest unadjusted p value occurred between dry-period PC2 and latitude ($p = 0.0437$; $q = 0.349$).

3.4. Environmental Relationships and Sensitivity Analyses

Before correction for multiple testing, several Fmax–TOC correlations were observed (Figure 6), but none of the 32 correlations in either period remained significant after BH correction; the lowest q values were 0.173 in the dry period and 0.0916 in the wet period.

The paired permutation tests found no dry–wet difference in any of the 32 component–environment correlations. The smallest exact p value was 0.200, and all adjusted q values were $\geq$0.898.

After normalization by bulk TOC, C2/TOC was lower in the wet period ($q = 0.0209$). C3/TOC was higher at the unadjusted level ($p = 0.0386$), but this difference did not remain significant after correction ($q = 0.0966$). Total Fmax/TOC did not differ ($q = 0.744$).

The dry-period C4 value at S2 was 3.03 times the next highest value and had a robust z score of 53.4. For this sample, rank 4 reduced EEM RMSE from 91.16 to 47.36. Removing the S2 pair strengthened rather than removed the protein-like compositional result; S2 was therefore retained in the primary analysis.

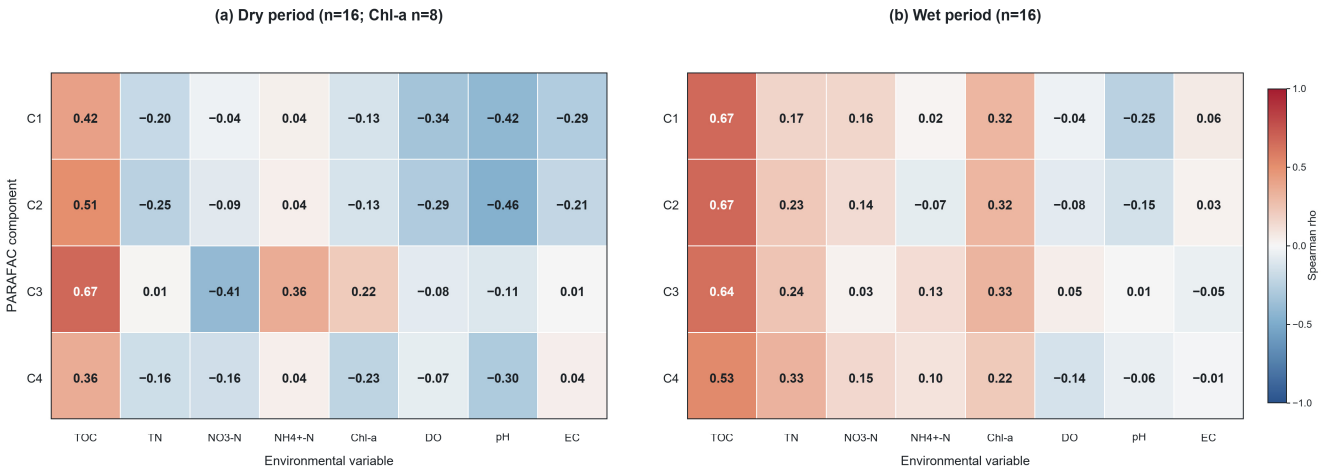


Figure 6. Spearman correlations between C1–C4 fluorescence intensities and eight environmental variables during (**a**) the dry period and (**b**) the wet period. Coefficients are shown without redundant plus signs. Sample size was $n = 16$ for each correlation except dry-period chlorophyll *a* ($n = 8$). No within-period correlation remained significant after BH correction, and exact within-site season-label permutation tests did not support a significant dry–wet difference in any of the 32 correlations.

4. Discussion

4.1. Seasonal Reorganization of Fluorescent Dom

The seasonal contrast was expressed more clearly in fluorescence composition than in total intensity. C2 Fmax and combined humic-like Fmax declined in the wet period, while total Fmax and bulk TOC showed no adjusted period difference. The protein-like contribution rose from 25.0% to 37.5%. Together with higher BIX, lower HIX, and unchanged FI, these results support a coherent FDOM compositional reorganization rather than a uniform change in bulk carbon.

The decoupling between bulk TOC and fluorescence composition indicates that seasonal changes in DOM quality can occur without a detectable change in the size of the bulk carbon pool. Such compositional shifts may influence DOM photoreactivity, microbial availability, and interactions with nutrients or contaminants, although these functional consequences were not measured directly in the present study [1,5].

The fluorescence indices and PCA support this composition-based interpretation. BIX increased and HIX decreased in the wet period, whereas FI remained unchanged. Possible mechanisms include changes in hydrological connectivity, terrestrial–aquatic exchange, mixing, and microbial processing under higher-water conditions; however, the present two-campaign design cannot separate these pathways or establish hydrological causality.

The magnitudes of FI, BIX, and HIX were not used for direct source-threshold or cross-study comparisons. These indices can be affected by instrument-response calibration, excitation and emission bandwidths, inner-filter effects, interpolation, and other preprocessing choices [8,10,11,38,41]. Because the archived workflow did not document instrument-response correction, Raman normalization, or absorbance-based inner-filter correction, the unusually high FI values cannot be compared quantitatively with calibrated values reported for Poyang Lake or other floodplain lakes. The defensible comparison is therefore limited to the internally paired direction of change: BIX increased, HIX decreased, and FI remained unchanged between the two campaigns.

Seasonal DOM patterns reported elsewhere in Poyang Lake are not uniform. Huang et al. [22], based on four hydrological periods, found more terrigenous CDOM and higher aromaticity in the rising and flood periods than in the dry and retreating periods, with different contributions from rivers and flooded wetlands among lake regions. Xu et al. [25]

also reported hydrologically structured changes in DOM chemistry using optical measurements and ultrahigh-resolution mass spectrometry. Our wet-period decrease in HIX and humic-like contribution differs from the dominant direction in those studies. This is not necessarily contradictory: sampling date, hydrological stage, sampled water masses, and analytical coverage can each alter the observed seasonal contrast. With only two campaigns and no synchronous site-specific water-level or discharge data, our results should be treated as campaign-specific rather than as a general wet-season response of Poyang Lake.

Regional PARAFAC studies likewise favor interpretation at the fluorescence-class level rather than by component number. Yan et al. [20] resolved three humic-like components and one protein-like component in size-fractionated organic matter from the five tributaries, whereas our model resolved two components in each broad class. Similar spectral labels do not establish that these solutions represent identical chemical pools. Xu et al. [24] combined optical spectroscopy with Fourier-transform ion cyclotron resonance mass spectrometry and found marked spatial heterogeneity and multiple DOM sources in Poyang Lake. Without comparable molecular or tracer evidence, our results support a decline in the humic-like share and a relative increase in the protein-like share, but not a source-specific assignment of C3 or C4.

4.2. Environmental Constraints and Sensitivity Analyses

The measured environmental variables did not identify a single explanation for the optical shift. Water temperature, pH, and TN differed between periods after multiple-testing correction, whereas the other measured variables did not. These concurrent changes cannot establish causation: the design contained only two temporal observations at each site and could not separate temperature, pH, nutrient, and other time-varying effects. Several Fmax–TOC correlations were nominally significant, particularly in the wet period, but none of the 32 within-period tests passed the Benjamini–Hochberg correction. Direct permutation tests also detected no dry–wet difference in correlation strength. The larger number of nominal correlations in the wet period therefore does not demonstrate stronger environmental coupling.

Normalization by TOC provided a more specific, but still limited, sensitivity test. C2/TOC declined in the wet period, whereas total Fmax/TOC remained unchanged. This pattern is compatible with a change in the fluorescent composition of the measured carbon pool rather than a uniform change in fluorescence per unit carbon. It is not a quantitative estimate of fluorophore yield: fluorescence–carbon relationships can vary with DOM composition and molecular size, and the carbon measurement here was bulk TOC whose filtration status could not be verified [10,52]. Fmax also remains in instrument-dependent arbitrary units because Raman normalization and instrument-response correction were not documented, so its magnitude should not be compared directly with values from other datasets [8,53]. Because absorbance-based inner-filter correction could not be verified, absolute interpretation of the fluorescence indices is also limited where inner-filter effects may occur [38,41]. Period-dependent inner-filter effects therefore cannot be excluded as a partial contributor to the observed optical differences. The paired comparisons are interpreted as operational differences within this dataset.

The PCA scores showed no adjusted relationship with latitude or longitude, but this does not imply spatial homogeneity. River channels, bays, open-lake waters, and seasonally inundated areas may influence DOM over distances that a simple coordinate gradient cannot represent. Hydrological studies have documented seasonally variable connections between lake and floodplain waters, while water-quality and DOM studies have reported pronounced spatial variation within Poyang Lake [16,17,22,24]. With 16 fixed sites and

no predefined hydrogeomorphic or land-use classes, our analysis could test only broad monotonic trends; it could not resolve local water masses or source zones.

The contrast with other monsoonal waters further argues against a single seasonal template. Ma et al. [14] found greater humification and aromaticity during the wet season in monsoonal rivers, together with a larger protein-like or autochthonous contribution during the dry season. Differences among studies may reflect hydrological connectivity, source mixtures, and sampling timing; Poyang Lake studies confirm that connectivity and water-quality patterns vary across hydrological settings [16,17]. In the absence of a synchronous site-scale hydrological dataset covering water level, discharge, rainfall, residence time, and inundation, those mechanisms cannot be tested here.

4.3. Model Uncertainty, Study Limitations, and Implications

The four-component PARAFAC solution is useful descriptively but is not fully validated at the component level. It fitted the EEMs better than the three-component model and was reproducible across random initializations, but its core consistency was low and only three of eight matched split-half comparisons met the strict excitation and emission congruence thresholds. Repeated convergence indicates numerical stability, not complete component resolution. Core consistency is one diagnostic rather than a stand-alone decision rule, and recent work indicates that it can be conservative for complex fluorescence data [43,54]. Fluorescence PARAFAC model selection should therefore consider fit, residuals, spectral plausibility, initialization stability, and split-half behavior together [6,42,44]. Rank 4 is retained as the better descriptive model, while agreement between ranks 3 and 4 on the direction of the combined humic-like and protein-like changes provides the more robust ecological result. The unusually high dry-period C4 value at S2 does not alter this class-level conclusion: rank 4 reconstructed its EEM more accurately, and excluding S2 strengthened rather than removed the period difference in protein-like proportion. Retaining S2 in the primary analysis and reporting the sensitivity analysis is therefore more transparent than excluding it based on its observed value.

The scope of inference is also constrained by the study design. The same 16 sites were sampled in two campaigns, without documented field or analytical replicates, and matched dry-period chl-*a* data were available at only eight sites. Daily Xingzi data establish contrasting monthly lake-level contexts, but synchronous site-level hydrological measurements and formal site classifications were unavailable.

Within these limits, the paired design detected a coherent change in fluorescent DOM composition even though bulk TOC and total Fmax showed no adjusted period difference. Composition-sensitive optical measurements may therefore complement bulk carbon concentration in seasonal monitoring, provided that analytical calibration, model validation, and multiplicity correction are reported explicitly. Future work should sample several hydrological stages across multiple years and include synchronous water level, discharge, rainfall, and residence-time indicators; absorbance-corrected, Raman-normalized EEMs; filtered DOC; analytical replicates; and independent molecular or source tracers. Such a design would test whether the observed compositional shift recurs and identify the hydrological or biogeochemical processes responsible for it.

5. Conclusions

The paired comparison across 16 fixed sites showed a coherent shift in fluorescent DOM between the dry- and wet-period campaigns. The four-component PARAFAC solution, used descriptively, resolved two humic-like and two protein-like fluorescence regions. C2 and combined humic-like Fmax were lower in the wet period, whereas bulk TOC and total Fmax did not differ after BH correction. At the same time, the mean protein-like

contribution increased from 25.0% to 37.5%, BIX increased, HIX decreased, and FI remained unchanged. An exact paired multivariate test also detected an overall difference across the optical variables. Fluorescence composition therefore showed a clearer campaign difference than did bulk TOC or total Fmax. Consequently, monitoring based only on bulk TOC may overlook environmentally relevant seasonal changes in DOM quality.

The observed optical shift does not identify a unique process, DOM source, or causal hydrological mechanism. The practical implication is that composition-sensitive fluorescence metrics can complement bulk TOC when monitoring seasonal DOM variation in large river-connected lakes. Resolving mechanisms will require multi-stage and multi-year sampling with synchronous hydrological observations, calibrated EEMs, filtered DOC, replication, and independent source tracers.

Author Contributions: Conceptualization, Y.Z. (Yiling Zhong) and H.L.; methodology, Y.Z. (Yiling Zhong); software, Y.Z. (Yiling Zhong), Y.S. and Z.H.; formal analysis, Y.Z. (Yiling Zhong); investigation, Y.Z. (Yiling Zhong), M.Z. and Y.Z. (Yuanyan Zhang); resources, H.L. and F.Y.; data curation, Y.Z. (Yiling Zhong); writing—original draft preparation, Y.Z. (Yiling Zhong); writing—review and editing, H.L. and F.Y.; visualization, Y.L.; supervision, H.L., F.Y. and Y.Z. (Yuanyan Zhang); project administration, Y.Z. (Yiling Zhong) and Y.Z. (Yuanyan Zhang); funding acquisition, H.L. All authors have read and agreed to the published version of the manuscript.

Funding: This research was funded by the Open Research Fund of Key Laboratory of Protection and Restoration of Yangtze River-connected Lake (Poyang Lake), Ministry of Ecology and Environment (PYHBX-Y-2025-05), and the National Key Research and Development Program Project (2024YFD1501004).

Institutional Review Board Statement: Not applicable.

Informed Consent Statement: Not applicable.

Data Availability Statement: Key statistical results are reported in the article. The archived raw EEM files, complete model-diagnostic outputs, and analysis code are available from the corresponding authors on reasonable request. Daily Xingzi-station water-level data used solely to characterize the hydrological context were provided by the Department of Ecology and Environment of Jiangxi Province and are not publicly available because of provider restrictions but can be made available confidentially to the editor and reviewers for verification.

Conflicts of Interest: The authors declare no conflicts of interest. The sponsors had no role in the design, execution, interpretation, or writing of the study.

References

1. Battin, T.J.; Luyssaert, S.; Kaplan, L.A.; Aufdenkampe, A.K.; Richter, A.; Tranvik, L.J. The boundless carbon cycle. *Nat. Geosci.* **2009**, *2*, 598–600. [CrossRef]
2. Tranvik, L.J.; Downing, J.A.; Cotner, J.B.; Loiselle, S.A.; Striegl, R.G.; Ballatore, T.J.; Dillon, P.; Finlay, K.; Fortino, K.; Knoll, L.B.; et al. Lakes and reservoirs as regulators of carbon cycling and climate. *Limnol. Oceanogr.* **2009**, *54*, 2298–2314. [CrossRef]
3. Stedmon, C.A.; Markager, S.; Bro, R. Tracing dissolved organic matter in aquatic environments using a new approach to fluorescence spectroscopy. *Mar. Chem.* **2003**, *82*, 239–254. [CrossRef]
4. Coble, P.G. Marine optical biogeochemistry: The chemistry of ocean color. *Chem. Rev.* **2007**, *107*, 402–418. [CrossRef] [PubMed]
5. Fellman, J.B.; Hood, E.; Spencer, R.G.M. Fluorescence spectroscopy opens new windows into dissolved organic matter dynamics in freshwater ecosystems: A review. *Limnol. Oceanogr.* **2010**, *55*, 2452–2462. [CrossRef]
6. Murphy, K.R.; Stedmon, C.A.; Graeber, D.; Bro, R. Fluorescence spectroscopy and multi-way techniques. PARAFAC. *Anal. Methods* **2013**, *5*, 6557–6566. [CrossRef]
7. Cory, R.M.; McKnight, D.M. Fluorescence spectroscopy reveals ubiquitous presence of oxidized and reduced quinones in dissolved organic matter. *Environ. Sci. Technol.* **2005**, *39*, 8142–8149. [CrossRef] [PubMed]
8. Murphy, K.R.; Butler, K.D.; Spencer, R.G.M.; Stedmon, C.A.; Boehme, J.R.; Aiken, G.R. Measurement of dissolved organic matter fluorescence in aquatic environments: An interlaboratory comparison. *Environ. Sci. Technol.* **2010**, *44*, 9405–9412. [CrossRef] [PubMed]

9. Ishii, S.K.L.; Boyer, T.H. Behavior of reoccurring PARAFAC components in fluorescent dissolved organic matter in natural and engineered systems: A critical review. *Environ. Sci. Technol.* **2012**, *46*, 2006–2017. [CrossRef] [PubMed]
10. Korak, J.A.; Dotson, A.D.; Summers, R.S.; Rosario-Ortiz, F.L. Critical analysis of commonly used fluorescence metrics to characterize dissolved organic matter. *Water Res.* **2014**, *49*, 327–338. [CrossRef] [PubMed]
11. Rosario-Ortiz, F.L.; Korak, J.A. Oversimplification of dissolved organic matter fluorescence analysis: Potential pitfalls of current methods. *Environ. Sci. Technol.* **2017**, *51*, 759–761. [CrossRef] [PubMed]
12. Miller, M.P.; McKnight, D.M. Comparison of seasonal changes in fluorescent dissolved organic matter among aquatic lake and stream sites in the Green Lakes Valley. *J. Geophys. Res. Biogeosci.* **2010**, *115*, G00F12. [CrossRef]
13. Zhao, Y.; Song, K.; Wen, Z.; Li, L.; Zang, S.; Shao, T.; Li, S.; Du, J. Seasonal characterization of CDOM for lakes in semiarid regions of Northeast China using excitation–emission matrix fluorescence and parallel factor analysis (EEM–PARAFAC). *Biogeosciences* **2016**, *13*, 1635–1645. [CrossRef]
14. Ma, Y.; Mao, R.; Li, S. Hydrological seasonality largely contributes to riverine dissolved organic matter chemical composition: Insights from EEM-PARAFAC and optical indicators. *J. Hydrol.* **2021**, *595*, 125993. [CrossRef]
15. Gelman, A.; Stern, H. The difference between "significant" and "not significant" is not itself statistically significant. *Am. Stat.* **2006**, *60*, 328–331. [CrossRef]
16. Wu, G.; Liu, Y. Seasonal water exchanges between China's Poyang Lake and its saucer-shaped depressions on river deltas. *Water* **2017**, *9*, 884. [CrossRef]
17. Li, Y.; Zhang, Q.; Cai, Y.; Tan, Z.; Wu, H.; Liu, X.; Yao, J. Hydrodynamic investigation of surface hydrological connectivity and its effects on the water quality of seasonal lakes: Insights from a complex floodplain setting (Poyang Lake, China). *Sci. Total Environ.* **2019**, *660*, 245–259. [CrossRef] [PubMed]
18. Yao, X.; Wang, S.; Ni, Z.; Jiao, L. The response of water quality variation in Poyang Lake (Jiangxi, People's Republic of China) to hydrological changes using historical data and DOM fluorescence. *Environ. Sci. Pollut. Res.* **2015**, *22*, 3032–3042. [CrossRef] [PubMed]
19. Xu, J.; Wang, Y.; Gao, D.; Yan, Z.; Gao, C.; Wang, L. Optical properties and spatial distribution of chromophoric dissolved organic matter (CDOM) in Poyang Lake, China. *J. Gt. Lakes Res.* **2017**, *43*, 700–709. [CrossRef]
20. Yan, C.; Liu, H.; Sheng, Y.; Huang, X.; Nie, M.; Huang, Q.; Baalousha, M. Fluorescence characterization of fractionated dissolved organic matter in the five tributaries of Poyang Lake, China. *Sci. Total Environ.* **2018**, *637–638*, 1311–1320. [CrossRef] [PubMed]
21. Wang, W.; Yang, P.; Xia, J.; Huang, H.Q.; Li, J. Impact of land use on water quality in buffer zones at different scales in the Poyang Lake, middle reaches of the Yangtze River basin. *Sci. Total Environ.* **2023**, *896*, 165161. [CrossRef] [PubMed]
22. Huang, Q.; Liu, L.; Huang, J.; Chi, D.; Devlin, A.T.; Wu, H. Seasonal dynamics of chromophoric dissolved organic matter in Poyang Lake, the largest freshwater lake in China. *J. Hydrol.* **2022**, *605*, 127298. [CrossRef]
23. Xu, J.; Jian, J.; Wang, Y.; Fang, C.; Hu, Q. Spatial-seasonal characteristics and influencing factors of dissolved organic carbon and chromophoric dissolved organic matter in Poyang Lake. *Environ. Earth Sci.* **2023**, *82*, 44. [CrossRef]
24. Xu, L.; Hu, Q.; Jian, M.; Mao, K.; Liu, Z.; Liao, W.; Yan, Y.; Shen, R.; Zhong, A. Exploring the optical properties and molecular characteristics of dissolved organic matter in a large river-connected lake (Poyang Lake, China) using optical spectroscopy and FT-ICR MS analysis. *Sci. Total Environ.* **2023**, *879*, 162999. [CrossRef] [PubMed]
25. Xu, L.; Hu, Q.; Liu, Z.; Jian, M.; Peng, Y.; Shen, R.; Liao, W.; Zhong, A. Hydrological alteration drives chemistry of dissolved organic matter in the largest freshwater lake of China (Poyang Lake). *Water Res.* **2024**, *251*, 121154. [CrossRef] [PubMed]
26. Huang, Q.; Liu, L.; Shah, L.; Wu, Y.; Wang, T.; Arhonditsis, G. Discriminating winter-drought and summer-flood regimes using CDOM optical proxies: A proof-of-concept analysis in Poyang Lake, China. *Water Res.* **2026**, *305*, 126474. [CrossRef] [PubMed]
27. Song, Y.; Zhang, Q.; Melack, J.M.; Li, Y. Groundwater dynamics of a lake-floodplain system: Role of groundwater flux in lake water storage subject to seasonal inundation. *Sci. Total Environ.* **2023**, *857*, 159414. [CrossRef] [PubMed]
28. Liu, H.; Zheng, L.; Jiang, L.; Liao, M. Forty-year water body changes in Poyang Lake and the ecological impacts based on Landsat and HJ-1 A/B observations. *J. Hydrol.* **2020**, *589*, 125161. [CrossRef]
29. Wang, L.; Liang, T. Distribution characteristics of phosphorus in the sediments and overlying water of Poyang Lake. *PLoS ONE* **2015**, *10*, e0125859. [CrossRef] [PubMed]
30. Li, Y.; Yao, J. Estimation of transport trajectory and residence time in large river–lake systems: Application to Poyang Lake (China) using a combined model approach. *Water* **2015**, *7*, 5203–5223. [CrossRef]
31. Lou, B.; Zhou, Z.; Su, H.; Zhuo, H. Temporal and spatial characteristics of key indicators of nutritional level and control standards in Lake Poyang. *J. Lake Sci.* **2023**, *35*, 897–908. [CrossRef]
32. Wu, Z.; Zhang, D.; Cai, Y.; Wang, X.; Zhang, L.; Chen, Y. Water quality assessment based on the water quality index method in Lake Poyang: The largest freshwater lake in China. *Sci. Rep.* **2017**, *7*, 17999. [CrossRef] [PubMed]
33. *HJ 501-2009*; Water Quality—Determination of Total Organic Carbon—Combustion Oxidation Nondispersive Infrared Absorption Method. China Environmental Science Press: Beijing, China, 2009.

34. *HJ 636-2012*; Water Quality—Determination of Total Nitrogen—Alkaline Potassium Persulfate Digestion UV Spectrophotometric Method. China Environmental Science Press: Beijing, China, 2012.
35. *HJ/T 346-2007*; Water Quality—Determination of Nitrate-Nitrogen—Ultraviolet Spectrophotometry (Trial). China Environmental Science Press: Beijing, China, 2007.
36. *HJ 535-2009*; Water Quality—Determination of Ammonia Nitrogen—Nessler's Reagent Spectrophotometry. China Environmental Science Press: Beijing, China, 2009.
37. State Environmental Protection Administration of China, Editorial Board of Water and Wastewater Monitoring and Analysis Methods. *Water and Wastewater Monitoring and Analysis Methods*, 4th ed.; China Environmental Science Press: Beijing, China, 2002; ISBN 7-80163-400-4.
38. Kothawala, D.N.; Murphy, K.R.; Stedmon, C.A.; Weyhenmeyer, G.A.; Tranvik, L.J. Inner filter correction of dissolved organic matter fluorescence. *Limnol. Oceanogr. Methods* **2013**, *11*, 616–630. [CrossRef]
39. McKnight, D.M.; Boyer, E.W.; Westerhoff, P.K.; Doran, P.T.; Kulbe, T.; Andersen, D.T. Spectrofluorometric characterization of dissolved organic matter for indication of precursor organic material and aromaticity. *Limnol. Oceanogr.* **2001**, *46*, 38–48. [CrossRef]
40. Huguet, A.; Vacher, L.; Relexans, S.; Saubusse, S.; Froidefond, J.-M.; Parlanti, E. Properties of fluorescent dissolved organic matter in the Gironde Estuary. *Org. Geochem.* **2009**, *40*, 706–719. [CrossRef]
41. Ohno, T. Fluorescence inner-filtering correction for determining the humification index of dissolved organic matter. *Environ. Sci. Technol.* **2002**, *36*, 742–746. [CrossRef] [PubMed]
42. Stedmon, C.A.; Bro, R. Characterizing dissolved organic matter fluorescence with parallel factor analysis: A tutorial. *Limnol. Oceanogr. Methods* **2008**, *6*, 572–579. [CrossRef]
43. Bro, R.; Kiers, H.A.L. A new efficient method for determining the number of components in PARAFAC models. *J. Chemom.* **2003**, *17*, 274–286. [CrossRef]
44. Andersen, C.M.; Bro, R. Practical aspects of PARAFAC modeling of fluorescence excitation-emission data: A review. *J. Chemom.* **2003**, *17*, 200–215. [CrossRef]
45. Coble, P.G. Characterization of marine and terrestrial DOM in seawater using excitation-emission matrix spectroscopy. *Mar. Chem.* **1996**, *51*, 325–346. [CrossRef]
46. Murphy, K.R.; Hambly, A.C.; Singh, S.; Henderson, R.K.; Baker, A.; Stuetz, R.; Khan, S.J. Organic matter fluorescence in municipal water recycling schemes: Toward a unified PARAFAC model. *Environ. Sci. Technol.* **2011**, *45*, 2909–2916. [CrossRef] [PubMed]
47. Chen, M.L.; Kim, S.-H.; Jung, H.-J.; Hyun, J.-H.; Choi, J.-H.; Lee, H.-J.; Huh, I.-A.; Hur, J. Dynamics of dissolved organic matter in riverine sediments affected by weir impoundments: Production, benthic flux, and environmental implications. *Water Res.* **2017**, *121*, 150–161. [CrossRef] [PubMed]
48. Sciscenko, I.; Arques, A.; Micó, P.; Mora, M.; García-Ballesteros, S. Emerging applications of EEM-PARAFAC for water treatment: A concise review. *Chem. Eng. J. Adv.* **2022**, *10*, 100286. [CrossRef]
49. Benjamini, Y.; Hochberg, Y. Controlling the false discovery rate: A practical and powerful approach to multiple testing. *J. R. Stat. Soc. Ser. B Stat. Methodol.* **1995**, *57*, 289–300. [CrossRef]
50. Korak, J.A.; McKay, G. Critical review of fluorescence and absorbance measurements as surrogates for the molecular weight and aromaticity of dissolved organic matter. *Environ. Sci. Processes Impacts* **2024**, *26*, 1663–1702. [CrossRef] [PubMed]
51. Chen, H.; Meng, W.; Zheng, B.H.; Wang, C.Y.; An, L.H. Optical signatures of dissolved organic matter in the watershed of a globally large river (Yangtze River, China). *Limnologica* **2013**, *43*, 482–491. [CrossRef]
52. Wu, F.C.; Kothawala, D.N.; Evans, R.D.; Dillon, P.J.; Cai, Y.R. Relationships between DOC concentration, molecular size and fluorescence properties of DOM in a stream. *Appl. Geochem.* **2007**, *22*, 1659–1667. [CrossRef]
53. Lawaetz, A.J.; Stedmon, C.A. Fluorescence intensity calibration using the Raman scatter peak of water. *Appl. Spectrosc.* **2009**, *63*, 936–940. [CrossRef] [PubMed]
54. Halberg, H.F.F.; Bevilacqua, M.; Rinnan, Å. Is core consistency a too conservative diagnostic? *J. Chemom.* **2023**, *37*, e3483. [CrossRef]

Disclaimer/Publisher's Note: The statements, opinions and data contained in all publications are solely those of the individual author(s) and contributor(s) and not of MDPI and/or the editor(s). MDPI and/or the editor(s) disclaim responsibility for any injury to people or property resulting from any ideas, methods, instructions or products referred to in the content.